Geophysical Research Letters

RESEARCH LETTER
10.1029/2024GL109623

Isotopic Constraints on Nitrous Oxide Emissions From the US Corn Belt

T. J. Griffis[1], Z. Yu[2], J. M. Baker[1,3], and D. B. Millet[1]

[1]Department of Soil, Water, and Climate, University of Minnesota-Twin Cities, Saint Paul, MN, USA, [2]Department of Natural Resources and Environmental Sciences, University of Illinois at Urban-Champaign, Urbana, IL, USA, [3]USDA-ARS Soil and Water Research Unit, Saint Paul, MN, USA

Key Points:

- Seasonality of N_2O isotope fingerprint driven by snowmelt and fertilizer input
- Snowmelt and growing season emissions dominated by nitrification versus denitrification pathways
- Isotope fingerprints were used to constrain direct and indirect N_2O emissions

Supporting Information:

Supporting Information may be found in the online version of this article.

Correspondence to:

T. J. Griffis and Z. Yu,
timgriffis@umn.edu;
zjyu@illinois.edu

Citation:

Griffis, T. J., Yu, Z., Baker, J. M., & Millet, D. B. (2024). Isotopic constraints on nitrous oxide emissions from the US Corn Belt. *Geophysical Research Letters*, *51*, e2024GL109623. https://doi.org/10.1029/2024GL109623

Received 5 APR 2024
Accepted 20 OCT 2024

Abstract Agriculture is the dominant source of anthropogenic nitrous oxide (N_2O) –a greenhouse gas and a stratospheric ozone depleting substance. The US Corn Belt is a large global N_2O source, but there remain large uncertainties regarding its source attribution and biogeochemical pathways. Here, we interpret high frequency stable N_2O isotope observations from a very tall tower to improve our understanding of regional source attribution. We detected significant seasonal variability in $\delta^{15}N_{bulk}$ (6.47–7.33‰) and the isotope site preference ($\delta^{15}N^{SP} = \delta^{15}N^{\alpha}–\delta^{15}N^{\beta}$, 18.22–25.19‰) indicating a predominance of denitrification during the growing period but of nitrification during the snowmelt period. Isotope mixing models and atmospheric inversions both indicate that indirect emissions contribute substantially (>35%) to total N_2O emissions. Despite the relatively large uncertainties, the upper bound of bottom-up indirect emission estimates are at the lower bound of the isotopic constraint, implying significant discrepancies that require further investigation.

Plain Language Summary Increasing use of synthetic nitrogen fertilizers for agricultural production is causing higher atmospheric nitrous oxide (N_2O) concentrations. Nitrous oxide is a long-lived greenhouse gas and degrades the protective stratospheric ozone layer. Using tall tower N_2O isotope observations from within the US Corn Belt, we examine how different processes (denitrification vs. nitrification) and sources (corn fields vs. wetlands, rivers, and streams) contribute to variations in atmospheric N_2O. The findings indicate that a substantial amount of nitrogen leakage from agricultural crops contributes to N_2O emissions via indirect sources such as drainage networks. These findings can help inform mitigation strategies targeting nitrogen use and leakage pathways from agricultural systems.

1. Introduction

Nitrous oxide (N_2O) is the third most important long-lived greenhouse gas and a major contributor to stratospheric ozone depletion (Montzka et al., 2011; Ravishankara et al., 2009). The most recent N_2O budget assessment suggests that global anthropogenic emissions (3.8 Tg N y^{-1}) increased by 30% from 1980 to 2016, with direct agricultural emissions accounting for up to 87% of the change (Tian et al., 2020). Over the same period, North American agricultural N_2O emissions are estimated to have increased from 0.38 to 0.58 Tg N y^{-1}. In the US Corn Belt, tall tower and airborne measurements combined with atmospheric inverse analyses suggest that emissions are 2 to 9-fold greater than bottom-up estimates (Chen et al., 2016; Del Grosso et al., 2022; Eckl et al., 2021; Griffis et al., 2013; Kort et al., 2008; Miller et al., 2012), implying large uncertainties in source contributions (e.g., from direct vs. indirect N_2O emissions, episodic emissions associated with freeze-thaw cycles and rain events) and in the underlying biogeochemical processes that regulate N cycling (Chen et al., 2016; Del Grosso et al., 2022; Hu et al., 2024; Turner et al., 2015). Direct agricultural N_2O emissions are derived from fertilized soils (predominantly crop fields in the Upper Midwestern United States), while indirect emissions are associated with deposition of reactive nitrogen volatilized from synthetic fertilizers and manure, leaching and runoff of fertilizer and manure N, and transport of terrestrially derived N_2O to streams via groundwater. It is now recognized that indirect N_2O emissions from leaching and runoff represents an important source of global emissions (Beaulieu et al., 2008, 2011). Further, a body of studies incorporating flux measurements from streams, stream modeling, and tall tower inverse analyses contend that direct N_2O emissions are well constrained and that indirect N_2O emissions have been underestimated in the Upper Midwest United States (Chen et al., 2016; Fu et al., 2018; Turner et al., 2015, 2016). However, recent work portends that direct N_2O emissions dominate (i.e., represent 94%) the regional budget (Lu et al., 2022) and that these emissions have been underestimated in regional assessments because poorly drained agricultural field observations have been inadequately represented

(Lawrence et al., 2021). These contrasting views, and large uncertainties, highlight the need for developing better constraints on regional N_2O emissions.

The N_2O molecule is linearly asymmetric ($N^{\beta} = N^{\alpha}$-O) with two stable N isotopes (^{14}N and ^{15}N) and three stable oxygen isotopes (^{16}O, ^{17}O, and ^{18}O) (Coplen, 2011). Measurements of these N_2O isotopes, including its isotopologues (e.g., $^{14}N^{14}N^{16}O$ and $^{15}N^{14}N^{16}O$) and isotopomers (e.g., $^{14}N^{15}N^{16}O$ and $^{15}N^{14}N^{16}O$), provide a useful tool to examine the origin and cycling mechanisms of N_2O (Ostrom & Ostrom, 2017; Toyoda et al., 2017; Yu, Harris, Henne, et al., 2020). By convention, the bulk N and O isotopic composition of N_2O is reported using delta (δ) notation ($\delta^{15}N_{bulk}$ and $\delta^{18}O$), where $\delta = (R_{sample}/R_{standard} - 1) \times 1{,}000$, reported in per mil (‰). The site-specific N isotope measurements of N_2O include $\delta^{15}N^{\alpha}$ and $\delta^{15}N^{\beta}$; the difference between these is the site preference ($\delta^{15}N^{SP} = \delta^{15}N^{\alpha} - \delta^{15}N^{\beta}$ (‰)) (Toyoda & Yoshida, 1999) and represents a powerful tracer for differentiating between oxidative and reductive N_2O formation pathways (i.e., nitrification and denitrification) as well as partial N_2O reduction (Toyoda et al., 2017).

Stable isotope measurements within the atmospheric boundary-layer (ABL) have the potential to improve our understanding of N_2O source attribution and partitioning (Harris et al., 2017, 2021, 2022) and have been applied broadly to other scalars including carbon dioxide (Bowling et al., 2001; Griffis, 2013) and water vapor (Griffis et al., 2016; Wang et al., 2010). Because microbial N_2O turnover is strongly controlled by environmental factors (e.g., N availability, temperature, and redox condition), N_2O emissions from different environmental niches and emission sectors can contain distinct isotopic signatures (Snider et al., 2015a, 2015b). For example, previous work has demonstrated that the global atmospheric $\delta^{15}N_{bulk}$ signal has decreased since 1940 because of increased use of synthetic N fertilizers and increased microbial activity that stimulate emissions of isotopically lighter N_2O (Park et al., 2012).

Our recent work based on extensive sampling in an agricultural river network within the US Corn Belt has shown that N_2O emissions from agricultural streams and rivers have significantly higher $\delta^{15}N^{SP}$ values (i.e., 22.5 ± 1.5‰) (Hu et al., 2024) than is typically found for direct soil N_2O emissions (i.e., 7.2 ± 3.8‰) (Snider, Thompson, et al., 2015; Wolf et al., 2015). These high $\delta^{15}N^{SP}$ values for stream-emitted N_2O are attributed to the delivery of soil-produced N_2O to streams via preferential flow paths draining soil macropores (e.g., pores associated with desiccation cracks, fissures, root channels, and earthworm burrows), where high oxygen availability may increase nitrification-based N_2O production compared to the bulk soil matrix (Hu et al., 2024; Yu et al., 2023). Therefore, measurements of N_2O isotopes in the ABL offer the potential for a powerful top-down constraint on sources and dynamics of N_2O emissions—beyond what can be obtained from bulk N_2O concentration measurements alone. However, due to technical challenges, few studies have measured N_2O isotopes at the high temporal resolution needed to characterize N_2O cycling complexity at landscape to regional scales—that is, the scales most pertinent to resolving anthropogenic and climatic controls on N_2O source variability (Butterbach-Bahl et al., 2013).

Recent laser spectroscopy advances have enabled the development of commercially available analyzers capable of resolving N_2O isotopologues and isotopomers at high time resolution (Clar & Anex, 2022; Harris et al., 2020). Harris et al. (2020) provide a comprehensive review of the available commercial analyzers, including performance characterization and workflow recommendations for reducing measurement artifacts and for improving data quality, reproducibility, and intercomparability. Here, we apply a cavity ring-down spectrometer (CRDS) to measure the isotope composition of N_2O ($\delta^{15}N_{bulk}$, $\delta^{15}N^{\alpha}$, $\delta^{15}N^{\beta}$, and $\delta^{15}N^{SP}$) in the ABL at the University of Minnesota Tall Tower Trace Gas Observatory (TGO)—a very tall tower (244 m) within the US Corn Belt. The N_2O isotope measurements are used to reveal processes contributing to regional N_2O emissions and to constrain N_2O emissions from characteristic high emission periods (e.g., those following snowmelt and fertilizer application) into direct and indirect pathways. The isotope partitioning approach is supported using independent scale factor Bayesian inverse analyses (SFBI) to examine which sources contribute most to the regional budget.

2. Methodology

2.1. Study Site

The N_2O isotope measurements described here were initiated in late summer 2022 at the University of Minnesota TGO (KCMP, radio tower, 44° 41′ 19″ N, 93° 40′ 22″ W; 290 m ASL), which is a 244 m communications tower (Griffis et al., 2017). TGO has been instrumented with meteorological and trace gas sensors since April 2007.

Carbon dioxide, water vapor, nitrous oxide, and methane (CH_4) are measured at sample heights of 100 and 185 m. The N_2O isotope air samples were collected at a height of 100 m above the ground surface using Teflon tubing (TPH0308-063 PFA 3/8″ID x 1/2″OD, Jensen Inert Products, Coral Springs, FL, USA). Teflon filter holders (12009-4m-147-4m pfa filter 47 mm x 1/4″MNPT x 1/4″MNPT Tefzel clamp, Jensen Inert Products) were installed at the inlets on the tower and before the sub-sample manifold located upstream of the N_2O analyzer. Sample lines were insulated with dense foam and heated using heat tape (Chromalox SRL, UT, USA) from the base of the tower to the manifold that was housed in a climate-controlled building to prevent condensation.

2.2. Isotope Measurement System

The isotope measurement system consists of a CRDS analyzer (model G5131-i, Picarro, Inc., Santa Clara, California, USA) and custom-built manifolds for routine air sampling and calibration. Figure S1 in Supporting Information S1 shows a schematic of the air sampling and calibration setup. The sampling system consisted of three manifolds (15481-4 EV/ET 4-Valve, Manifold, #10–32, Clippard, Cincinnati, OH, USA) and 9 valves (EV-2M-12; Way Electric Valve, Normally Closed, Manifold Mount, Wire Leads, 12 VDC, Clippard, Cincinnati, OH, USA). Two manifolds were used for online mixing and delivering calibration isotope standards and for quantifying the effects of CH_4 interference. One manifold was used for introducing the calibration gas matrix, a long-term check tank (ambient) standard, and the tall tower 100 m air subsample to the CRDS analyzer. Three mass flow controllers (MC-50SCCM-D, Alicat Scientific Inc., Tucson, Arizona, USA) were used for automated span gas calibration and for setting the base subsample flow for the CRDS analyzer. Automated valve switching and control of the mass flow controllers was performed using a data logger (CR5000, Campbell Scientific Inc., Logan, Utah, USA). All data were archived using the CR5000 and CRDS computer system at 0.4 Hz.

2.3. Preparation and Measurement of Calibration Gases

A detailed description of the preparation and measurement of calibration gases is provided in the Supporting Information (Text S1 in Supporting Information S1). Briefly, we prepared three calibration gases (i.e., Cal 1 to 3) in 29.5 L aluminum cylinders by diluting N_2O isotope reference materials, USGS51 and USGS52 (Ostrom et al., 2018), and a newly established reference material, RM3A (Mohn et al., 2022) (Table S1a in Supporting Information S1) using purified dry ambient air. As a result, the prepared calibration gases have different N_2O isotope composition than the parent reference materials but contain CH_4 at ambient level, which minimizes correction for the CH_4 interference effect (Harris et al., 2020). The prepared calibration gases were subsampled and measured for $\delta^{15}N_{bulk}$, $\delta^{18}O$, $\delta^{15}N^{\alpha}$, $\delta^{15}N^{\beta}$, and $\delta^{15}N^{SP}$ using an isotope ratio mass spectrometer (Elementar Isoprime precision, Germany) coupled with a preconcentration unit (Elementar iso FLUX GHG, Germany). These measurements were calibrated using undiluted USGS51, USGS52, and RM3A. The final calibration values of the three calibration gases are shown in Table S1b in Supporting Information S1.

2.4. Tall Tower Sampling and Isotope Calibration

The tall tower 100 m inlet was subsampled continuously for two 11-hr periods each day that were bookended by calibration periods. A 1-hr calibration cycle was performed twice per day (0230 and 1430 LST) and consisted of the following steps: (a) a "check tank" filled with ambient air was first sampled for 8 min to correct any measurement drift prior to calibration; (b) standard cylinder Cal 1 was then sampled for 8 min; (c) standard cylinder Cal 2 was sampled for 8 min; (d) standard cylinder Cal 3 was sampled using three different ultra zero air dilutions optimized to bracket the ambient N_2O mixing ratio. Each Cal 3 dilution was sampled for 8 min, and combined, these measurements of diluted Cal 3 were used to correct for any potential dependence of the isotope measurements on N_2O concentration. The remaining time within the 1-hr calibration cycle was used to re-sample the check tank. The tall tower 100 m inlet subsampling then resumed until the next calibration cycle. Figure S2 in Supporting Information S1 provides an example of the air sample and calibration routine, showing a long-term (several days) and a magnified (~1 day) view. A description of the post processing routine is provided in the Supporting Information (Text S2 in Supporting Information S1).

2.5. Isotopic Constraints on Emission Sources

A Miller-Tans mixing model (SI Text 3) was used with the tall tower N_2O isotope observations to estimate the isotope composition of the regional net N_2O emissions ($F\delta^{15}N$ and $F\delta^{15}N^{SP}$) during the growing season (J. B.

Miller & Tans, 2003). We did not use measured $\delta^{18}O$ values for this analysis because the inherent complexity of oxygen isotope exchange reactions during N_2O production makes the $\delta^{18}O$ source signatures of N_2O less well quantified compared to $\delta^{15}N_{bulk}$ and $\delta^{15}N^{SP}$ (Lewicka-Szczebak et al., 2016). Similar mixing model approaches (e.g., Keeling plot, flux ratio plot) have been used to estimate the isotope composition of CO_2 and water vapor exchange at the same tall tower site (Griffis et al., 2010, 2016; Keeling, 1958). Here, the mixing line analysis was applied to relatively high frequency intervals (i.e., every 15 min; 30 min; 1 hr; 3 hr; 6 hr; etc.) for each day. This multi-timescale approach was applied to help assess the uncertainty in estimating the isotope composition of net N_2O emissions (Figure S9 in Supporting Information S1). The mixing line analysis was restricted to the snowmelt and growing season period when N_2O emissions were sufficiently large to enhance the signal (i.e., buildup) of ABL N_2O. The end member estimates from the Miller-Tans approach were filtered from further analysis if they exceeded the range of individual source signatures reported in the literature (Table S2 in Supporting Information S1) and when the regression correlation coefficient was less than 0.5. From Figure S9 in Supporting Information S1, we used the median values and uncertainty (95% confidence intervals) within a Monte Carlo approach to partition the net regional N_2O emissions into direct versus indirect emissions (described below).

The isotope composition of regional emissions and end member values for direct (i.e., emissions from fertilized farm fields) and indirect (defined here as the offsite emissions associated with leaching and runoff) N_2O emissions (Table S2 in Supporting Information S1) were used within a simple two-member isotope mixing model to determine the relative partitioning between these two major source types. A Monte Carlo approach allowed random sampling (n = 100,000 iterations) from the distribution of the isotope end members (Table S2 in Supporting Information S1) and isotope composition of the net flux (Figure S9 in Supporting Information S1). In this way, the isotope partitioning approach accounted for the uncertainty in the isotope composition of the regional net flux and associated end members. This isotope partitioning result was then compared with an atmospheric inverse modeling approach, described below.

2.6. Atmospheric Inverse Analyses

Following our previous work, we used the tall tower hourly observations (100 m level) within a SFBI approach (Chen et al., 2016; Kim et al., 2013) to constrain the regional N_2O budget and to estimate direct and indirect emissions during spring 2023. Previously published results for 2010–2015 derived using the same methodology (Griffis et al., 2017) are also reported here to provide context for the 2023 findings. The salient details of the SFBI approach are provided in the supporting information (Text S4 in Supporting Information S1).

3. Results and Discussion

3.1. Isotope Composition of the Atmospheric Boundary-Layer

The seasonality of the N_2O isotope composition and "clean air" values are summarized in Figure 1. Examining all valid daytime and nighttime data collected over the measurement period (DOY 1 to DOY 360, 2023) we find median (±1 s.e. of the median) values of: N_2O = 342.48 (±0.06) nmol mol^{-1}, $\delta^{15}N^{\alpha}$ = +18.94 (±0.05)‰, $\delta^{15}N^{\beta}$ = −3.67 (±0.03)‰, $\delta^{15}N_{bulk}$ = 7.33 (±0.03)‰ and $\delta^{15}N^{SP}$ = 22.65 (±0.12)‰ (Figure 1). These values differ substantially from global (i.e., background) values, 336.58 nmol mol^{-1}, +15.8, −2.3, 6.45, and 18.1‰, respectively (Ghosh et al., 2023; Liang et al., 2022; Park et al., 2012) and recent (July 2014 to February 2016) measurements reported for Dübendorf, Switzerland (Harris et al., 2017). These differences may be driven by regional circulation patterns over the 1-year measurement period and by variations in sources and biogeochemical pathways contributing to the N_2O signal. We estimated clean air (i.e., low source emission conditions) values as the lower tenth percentile of all N_2O observations. These values were: N_2O = 338.09 (±0.02) nmol mol^{-1}, $\delta^{15}N^{\alpha}$ = +16.6 (±0.07)‰, $\delta^{15}N^{\beta}$ = −2.44 (±0.10)‰, $\delta^{15}N_{bulk}$ = 6.88 (±0.07)‰ and $\delta^{15}N^{SP}$ = 19.05 (±0.12)‰ and were in better agreement with the global background values. Below, we show how these signals vary across different temporal scales, which allows interpretation of systematic changes more carefully as the results are not affected by potential offsets between laboratories.

Freeze-thaw conditions are an important driver of global N_2O emissions (Wagner-Riddle et al., 2017). The snowmelt period (approximately DOY 50 to DOY 100) has been associated with significant N_2O emissions in the Upper Midwestern United States, accounting for about 35% of the annual budget (Griffis et al., 2017). Median snowmelt values were: N_2O = 341.83 (±0.07) nmol mol^{-1}, $\delta^{15}N^{\alpha}$ = 19.91 (±0.06)‰, $\delta^{15}N^{\beta}$ = −4.73 (±0.13)‰, $\delta^{15}N_{bulk}$ = 7.25 (±0.06)‰, and $\delta^{15}N^{SP}$ = 25.19 (±0.20)‰, respectively. The relatively large increase in $\delta^{15}N^{SP}$

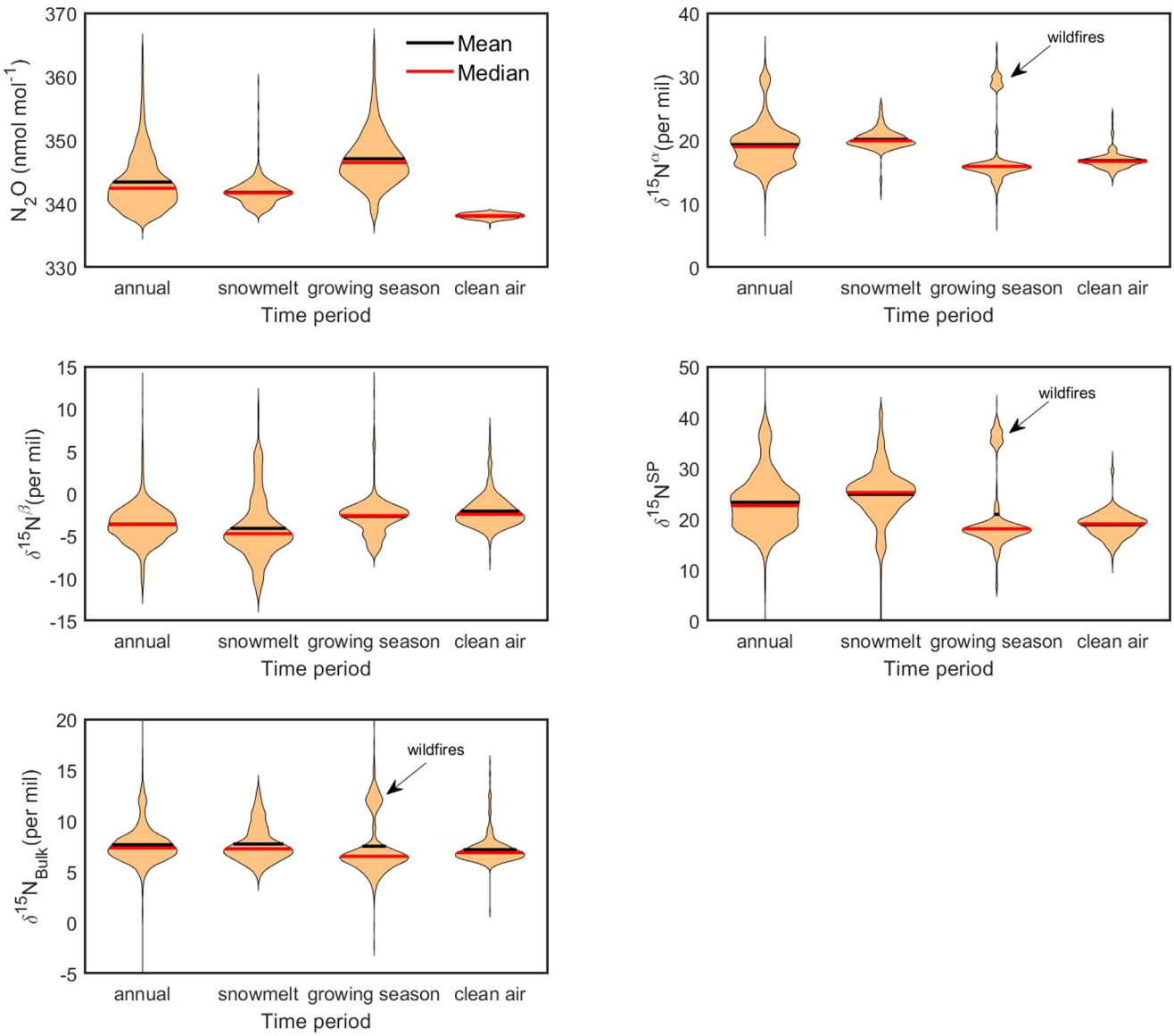

Figure 1. Seasonal changes in the N_2O isotope composition of the atmospheric boundary-layer at the University of Minnesota Tall Tower Trace Gas Observatory in 2023. Also shown are "clean air" values estimated as the lower tenth percentile of the N_2O concentrations. Note that some extreme outliers are revealed in the violin plots that were associated with advection of smoke from Canadian wildfires including events on DOY 132 to DOY 143 and DOY 170 to DOY 176.

(2.5‰ higher than annual values; 6.1‰ higher than clean air values) and the small change in $\delta^{15}N_{bulk}$ relative to the annual or clean air values implies that there was enhanced nitrification during the snowmelt period. It is well established that nitrification causes elevated $\delta^{15}N^{SP}$ whereas denitrification acts to lower $\delta^{15}N^{SP}$ (Toyoda et al., 2017). Here, we hypothesize that microbial cell lysis during snowmelt released labile organic compounds that promoted rapid mineralization followed by nitrification. Cao et al. (2023) have shown that snowmelt N_2O emissions were highly correlated with the presence of the nitrification genes amoA and amoB, supporting the hypothesis that nitrification dominates N_2O production during these periods.

Large regional emissions (55% of the annual budget) have also been associated with the early to mid-growing period (DOY 150 to DOY 200) following fertilizer application (Griffis et al., 2017). The median values during this period were: N_2O = 346.57 (±0.15) nmol mol^{-1}, $\delta^{15}N^{\alpha}$ = +15.92 (±0.21)‰, $\delta^{15}N^{\beta}$ = −2.68 (±0.09)‰, $\delta^{15}N_{bulk}$ = 6.47 (±0.11)‰, and $\delta^{15}N^{SP}$ = 18.22 (±0.28)‰. These values indicate substantial enhancement of the N_2O mixing ratios driven by regional emissions. The relative depletion of $\delta^{15}N^{\alpha}$ (i.e., a decrease of ~3‰,

0.68‰), $\delta^{15}N^{SP}$ (i.e., a decrease of ~4.4‰, 0.80‰), and $\delta^{15}N_{bulk}$ (i.e., a decrease of ~1‰, 0.41‰), when compared to the annual or clean air values, is consistent with the contribution of N_2O emissions derived from relatively ^{15}N depleted sources. The isotope composition of N_2O emissions derived from agricultural soils and rivers have been shown to be depleted in the heavy isotopes, leading to isotopically light ABL concentrations (Table S2 in Supporting Information S1). For example, the bacterial denitrification pathway is associated with strong kinetic fractionation resulting in isotopically depleted emissions (e.g., $\delta^{15}N_{bulk}$ ranges from −50‰ to +5‰) and a $\delta^{15}N^{SP}$ value near 0‰ (Sutka et al., 2006; Toyoda et al., 2017; Yu, Harris, Lewicka-Szczebak, et al., 2020).

During summer 2023, Canadian wildfires significantly impacted air quality in Minnesota (Figure S9 in Supporting Information S1). We observed that biomass burning exerted a significant influence on the isotope composition of N_2O and that these variations correlated with large increases in the EPA-reported air quality index (AQI). From DOY 132 to DOY 143, N_2O mixing ratios were significantly elevated and enriched in ^{15}N relative to background air (Figure S9 in Supporting Information S1). The median values were: N_2O = 343.79 (±0.003) nmol mol^{-1}, $\delta^{15}N^{\alpha}$ = +19.50 (±0.006)‰, $\delta^{15}N^{\beta}$ = −3.97 (±0.006)‰, $\delta^{15}N_{bulk}$ = 7.55 (±0.005)‰, and $\delta^{15}N^{SP}$ = 23.96 (±0.008)‰. Similarly, over the period DOY 170 to DOY 176, we observed elevated values associated with the advection of wildfire smoke into the region and relatively high AQI values. The median values were: N_2O = 346.83 (±0.01) nmol mol^{-1}, $\delta^{15}N^{\alpha}$ = +29.08 (±0.03)‰, $\delta^{15}N^{\beta}$ = −5.26 (±0.03)‰, $\delta^{15}N_{bulk}$ = 12.21 (±0.03)‰, and $\delta^{15}N^{SP}$ = 36.04 (±0.04)‰. These wildfire outliers are evident in the violin plots shown in Figure 1. The influence of biomass burning on N_2O isotope composition has not been thoroughly studied. Agricultural biomass burning experiments, conducted under controlled laboratory conditions, have demonstrated relative small impacts on the isotope composition of N_2O (Table S2 in Supporting Information S1) with $\delta^{15}N_{bulk}$ signatures that were depleted in ^{15}N relative to that of crop residue N (Ogawa & Yoshida, 2005). However, key differences in nitrogen substrate in forests and variations in fire temperature under field conditions could substantially influence the extent of isotope effects during N_2O production and thermal destruction.

3.2. Isotope Composition of Regional N_2O Emissions

Here, we present three estimates of the isotope composition of regional N_2O emissions. First, the a priori isotope composition of the regional N_2O emissions was estimated from the WRF-STILT source footprint modeling, N_2O emission inventory data, and the mean isotope composition of these sources (Table S2 in Supporting Information S1, Figure 2). This simple footprint-weighted estimate was performed April through September in 2016, 2019, and 2023. These footprint-weighted calculations resulted in a priori $F\delta^{15}N$ and $F\delta^{15}N^{SP}$ median values of −16.95 (±1 s.e. of the median, ±0.02)‰ and 13.72 (±0.16)‰, respectively. Figure 2 shows these footprint-weighted values relative to other key sources.

Second, the isotope composition of regional N_2O emissions was constrained for the snowmelt and growing season using the Miller-Tans mixing model approach. The $F\delta^{15}N$ and $F\delta^{15}N^{SP}$ median values for the entire period were −11.1‰ (±1 s.e. of the median, 1.0‰) and 17.0‰ (±1.4‰) (Figure S10 in Supporting Information S1). These values are similar to, or near the limits of, recent global source estimates (−12.0 to −10.0‰ and 8.5 to 18‰, respectively) derived from long-term isotopic observations and global budget analyses (Ghosh et al., 2023; Park et al., 2012; Yu, Harris, Henne, et al., 2020). Deviations from the global values are expected given the intense agricultural production and fertilizer use within the region and, therefore, increased denitrification/nitrification where microbial activity favors the lighter isotopes.

Finally, we estimated the a posteriori isotope composition of regional N_2O emissions based on the combination of the optimized SFBI analyses and the reported isotope end members (Table S2 in Supporting Information S1) from mass balance considerations. Here, a similar Monte Carlo approach was used to sample from within each respective sample distribution (i.e., direct and indirect emissions from SFBI and isotope end members). These analyses indicate that the simulated $F\delta^{15}N$ and $F\delta^{15}N^{SP}$ median values were −16.6‰ (±0.02‰) and 15.7‰ (±0.02‰), respectively (Figure S11 in Supporting Information S1). These values are within the range of estimates determined using the tall tower observations and mixing line analyses and similar to the footprint-weighted modeling (a priori) values. However, the optimized $F\delta^{15}N^{SP}$ values were approximately 2‰ higher than the a priori values, implying a larger contribution from the indirect N_2O emissions. Figure 2 supports that the tall tower N_2O isotope fingerprints depart appreciably from the global source values with regional $F\delta^{15}N$ values approximately 6‰ lower and $F\delta^{15}N^{SP}$ weighted toward indirect emissions associated with leaching and runoff.

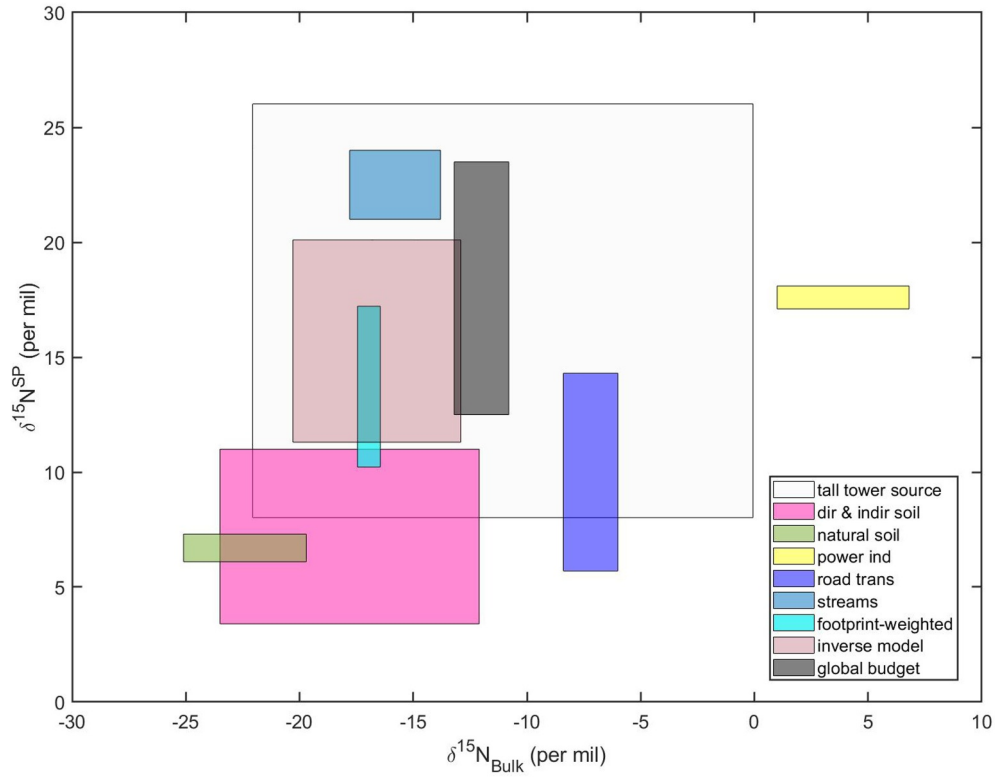

Figure 2. Isotope composition of N_2O emissions from different sources including regional estimates based on tall tower observations and global budget analyses. The three tower-based estimates include: 1. Simple footprint-weighted estimate (footprint-weighted); 2. Isotope mixing line analyses (tall tower source estimate); and 3. A posteriori estimate based on atmospheric inverse analyses (inverse model). The three tall tower estimates are for the snowmelt to early growing season period. Note that all estimates shown are based on nominal values and their standard deviation. The footprint-weighted estimate is based on the nominal end member values and the overall uncertainty is represented as the range of computed values.

Using the Monte Carlo isotope mixing model approach, we constrained the relative partitioning of N_2O emissions (Figure 3). The $F\delta^{15}N$ and $F\delta^{15}N^{SP}$ mixing models yielded different partitioning results. Partitioning based on $F\delta^{15}N^{SP}$ indicates that indirect N_2O emissions during the 2023 growing season were 64% (IQR = 51–75%) of total emissions. This relatively large indirect emission estimate might be caused by an $F\delta^{15}N^{SP}$ end member value that is weighted toward a nitrification signal or stems from underrepresentation of regional watersheds. The $F\delta^{15}N$ partitioning indicates that indirect emissions accounted for about 35% (IQR = 20%–55%), which represents the upper bound of current bottom-up inventory estimates (25%–30%) (Chen et al., 2016). Both estimates are substantial, but exhibit relatively large uncertainties, bracketing the estimates derived from atmospheric inverse analyses (Figure 3) for 2023 and for the period 2010 to 2015. For example, in spring 2023, the SFBI analyses yielded a partitioning of 47.8 Gg N_2O–N and 48.4 Gg N_2O–N for direct and indirect emissions, respectively. Multi-year monthly SFBI analyses suggest that indirect emissions accounted for 41%–58% of agricultural emissions (Chen et al., 2016; Griffis et al., 2017).

These independent lines of evidence (e.g., multiple isotope fingerprints and SFBI analyses) suggest that indirect N_2O emissions represent a substantial component (at least 35%) of regional emissions. However, the uncertainties associated with source partitioning based on isotope observations or SFBI analyses remains very large (>100%). New efforts are currently underway within the US Corn Belt to expand tall tower observations, as well as bottom-up direct and indirect flux measurements using eddy covariance and chamber observations. These new observations are being made possible through the United States Inflation Reduction Act (https://www.whitehouse.gov/wp-content/uploads/2023/11/NationalGHGMMISStrategy-2023.pdf) and offer a new opportunity to improve constraints on regional top-down N_2O emissions and the upscaling of direct/indirect emissions. Further, we propose that improved observations of the N_2O isotope end members in combination with a dual isotope inverse

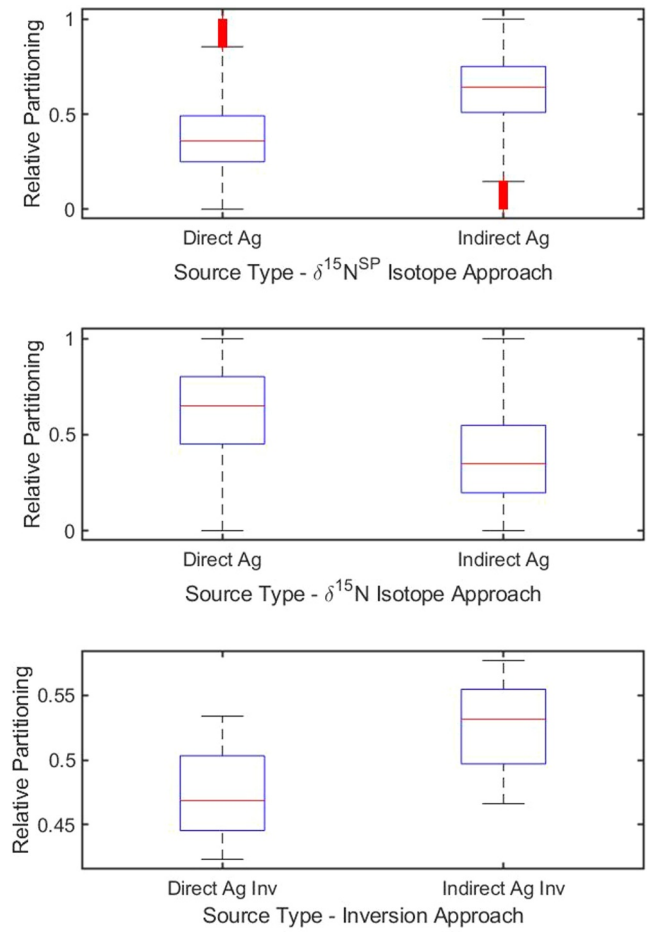

Figure 3. Constraining regional N_2O emissions into direct versus indirect emissions using independent isotope tracers ($\delta^{15}N_{Bulk}$ and $\delta^{15}N^{SP}$) and scale factor Bayesian inverse analyses. The isotope partitioning is shown for the growing season of 2023. The inverse analyses are based on previously published values from 2010 to 2015 (Chen et al., 2016; Griffis et al., 2017).

modeling approach could provide improved constraints on N_2O source attribution. We expect these new research efforts will help reduce the large uncertainties associated with regional N_2O partitioning.

4. Conclusions

The isotope composition of N_2O was measured at the University of Minnesota Tall Tower Trace Gas Observatory over an annual cycle using a cavity ring-down spectroscopy technique. Seasonal variations in the isotope signals were associated with the snowmelt and early growing season periods. The changes in $\delta^{15}N_{bulk}$ and $\delta^{15}N^{SP}$ showed relative depletion in the heavier isotopes during the early growing season, which is consistent with emissions associated with agricultural sources. The seasonal variability in $\delta^{15}N_{bulk}$ and $\delta^{15}N^{SP}$ indicated a predominance of denitrification during the growing period but of nitrification during the snowmelt period. Multiple approaches were used to differentiate between the two major N_2O sources including direct and indirect emissions. Scale factor Bayesian inverse analyses and two different N_2O isotope fingerprints suggest that indirect emissions can account for 35%–64% (mean of 51%) of the snowmelt and growing season budget. We find that the upper bound of bottom-up indirect emission estimates are at the lower bound of the isotopic constraint.

Data Availability Statement

The data set (Tall Tower N2O Isotopes 2023; Griffis et al., 2024) presented here is publicly available and will be published at ESS-DIVE (Deep Insights for Earth Science Data).

Acknowledgments
This work was supported by grants from the US National Science Foundation (projects 2110241 and 2110430). We thank Alex Frie and Ke Xiao for their technical assistance with the transport models used in this study. The University of Minnesota Supercomputing Institute (https://www.msi.umn.edu/) provided computational support for the atmospheric transport modeling. Calibration of N_2O isotopes was realized as part of a Transnational Access project supported by the European Commission under the Horizon 2020—Research and Innovation Framework Programme, H2020-INFRAIA-2020-1, ATMO-ACCESS Grant Agreement number: 101008004. We thank Dr. Joachim Mohn, Empa, Laboratory for Air Pollution/ Environmental Technology, Dübendorf, Switzerland, for providing calibration materials, advice, and comments on an early draft of this manuscript.

References

Beaulieu, J. J., Arango, C. P., Hamilton, S. K., & Tank, J. L. (2008). The production and emission of nitrous oxide from headwater streams in the Midwestern United States. *Global Change Biology*, *14*(4), 878–894. https://doi.org/10.1111/j.1365-2486.2007.01485.x

Beaulieu, J. J., Tank, J. L., Hamilton, S. K., Wollheim, W. M., Hall, R. O. Jr., Mulholland, P. J., et al. (2011). Nitrous oxide emission from denitrification in stream and river networks. *Proceedings of the National Academy of Sciences of the United States of America*, *108*(1), 214–219. https://doi.org/10.1073/pnas.1011464108

Bowling, D. R., Tans, P. P., & Monson, R. K. (2001). Partitioning net ecosystem carbon exchange with isotopic fluxes of CO_2. *Global Change Biology*, *7*(2), 127–145. https://doi.org/10.1046/j.1365-2486.2001.00400.x

Butterbach-Bahl, K., Baggs, E. M., Dannenmann, M., Kiese, R., & Zechmeister-Boltenstern, S. (2013). Nitrous oxide emissions from soils: How well do we understand the processes and their controls? *Philosophical Transactions of the Royal Society B: Biological Sciences*, *368*(1621), 20130122. https://doi.org/10.1098/rstb.2013.0122

Cao, X., Liu, H., Liu, Y., Jing, J., Wen, L., Xu, Z., et al. (2023). N_2O emission associated with shifts of bacterial communities in riparian wetland during the spring thawing periods. *Ecology and Evolution*, *13*(3), e9888. https://doi.org/10.1002/ece3.9888

Chen, Z., Griffis, T. J., Millet, D. B., Wood, J. D., Lee, X., Baker, J. M., et al. (2016). Partitioning N_2O emissions within the US Corn Belt using an inverse modeling approach. *Global Biogeochemical Cycles*, *30*(8), 1192–1205. https://doi.org/10.1002/2015GB005313

Clar, J. T. F., & Anex, R. P. (2022). Assessing nitrous oxide (N_2O) isotopic analyzer performance for in-field use. *Agricultural and Forest Meteorology*, *316*, 108855. https://doi.org/10.1016/j.agrformet.2022.108855

Coplen, T. (2011). Guidelines and recommended terms for expression of stable-isotope-ratio and gas-ratio measurement results. *Rapid Communications in Mass Spectrometry*, *25*(17), 2538–2560. https://doi.org/10.1002/rcm.5129

Del Grosso, S. J., Ogle, S. M., Nevisonc, C., Gurung, R., Parton, W. J., Wagner-Riddle, C., et al. (2022). A gap in nitrous oxide emission reporting complicates long-term climate mitigation. *Proceedings of the National Academy of Sciences of the United States of America*, *119*(31), e2200354119. https://doi.org/10.1073/pnas.2200354119

Eckl, M., Roiger, A., Kostinek, J., Fiehn, A., Huntrieser, H., Knote, C., et al. (2021). Quantifying nitrous oxide emissions in the US midwest: A top-down study using high resolution airborne in-situ observations. *Geophysical Research Letters*, *48*(5). https://doi.org/10.1029/2020GL091266

Fu, C., Lee, X., Griffis, T. J., Baker, J. M., & Turner, P. A. (2018). A modeling study of direct and indirect N_2O emissions from a representative catchment in the U.S. Corn Belt. *Water Resources Research*, *54*(5), 3632–3653. https://doi.org/10.1029/2017WR022108

Ghosh, S., Toyoda, S., Buizert, C., Etheridge, D. M., Langenfelds, R. L., Yoshida, N., et al. (2023). Concentration and isotopic composition of atmospheric N_2O over the last century. *Journal of Geophysical Research: Atmospheres*, *128*(12), e2022JD038281. https://doi.org/10.1029/2022JD038281

Griffis, T. J. (2013). Tracing the flow of carbon dioxide and water vapor between the biosphere and atmosphere: A review of optical isotope techniques and their application. *Agricultural and Forest Meteorology*, *174–175*, 85–109. https://doi.org/10.1016/j.agrformet.2013.02.009

Griffis, T. J., Baker, J. M., Sargent, S. D., Erickson, M., Corcoran, J., Chen, M., & Billmark, K. (2010). Influence of C_4 vegetation on $^{13}CO_2$ discrimination and isoforcing in the Upper Midwest, United States. *Global Biogeochemical Cycles*, *24*(4), GB4006. https://doi.org/10.1029/2009GB003594

Griffis, T. J., Chen, Z., Baker, J. M., Wood, J. D., Millet, D. B., Lee, X., et al. (2017). Nitrous oxide emissions are enhanced in a warmer and wetter world. *Proceedings of the National Academy of Sciences of the United States of America*, *114*(45), 12081–12085. https://doi.org/10.1073/pnas.1704552114

Griffis, T. J., Lee, X., Baker, J. M., Russelle, M. P., Zhang, X., Venterea, R., & Millet, D. B. (2013). Reconciling the differences between top-down and bottom-up estimates of nitrous oxide emissions for the US Corn Belt. *Global Biogeochemical Cycles*, *27*(3), 746–754. https://doi.org/10.1002/gbc.20066

Griffis, T. J., Wood, J. D., Baker, J. M., Lee, X., Xiao, K., Chen, Z., et al. (2016). Investigating the source, transport, and isotope composition of water vapor in the planetary boundary layer. *Atmospheric Chemistry and Physics*, *16*(8), 5139–5157. https://doi.org/10.5194/acp-16-5139-2016

Griffis, T. J., Yu, Z., Baker, J. M., & Millet, D. B. (2024). Tall tower N2O isotopes 2023. Retrieved from https://biometeorology.umn.edu/n2o-isotope

Harris, E., Diaz-Pines, E., Stoll, E., Schloter, M., Schulz, S., Duffner, C., et al. (2021). Denitrifying pathways dominate nitrous oxide emissions from managed grassland during drought and rewetting. *Science Advances*, *7*(6). https://doi.org/10.1126/sciadv.abb7118

Harris, E., Henne, S., Huglin, C., Zellweger, C., Tuzson, B., Ibraim, E., et al. (2017). Tracking nitrous oxide emission processes at a suburban site with semicontinuous, in situ measurements of isotopic composition. *Journal of Geophysical Research: Atmospheres*, *122*(3), 1850–1870. https://doi.org/10.1002/2016JD025906

Harris, E., Yu, L., Wang, Y.-P., Mohn, J., Henne, S., Bai, E., et al. (2022). Warming and redistribution of nitrogen inputs drive an increase in terrestrial nitrous oxide emission factor. *Nature Communications*, *13*(1), 4310. https://doi.org/10.1038/s41467-022-32001-z

Harris, S. J., Liisberg, J., Xia, L., Wei, J., Zeyer, K., Yu, L., et al. (2020). N_2O isotopocule measurements using laser spectroscopy: Analyzer characterization and intercomparison. *Atmospheric Measurement Techniques*, *13*(5), 2797–2831. https://doi.org/10.5194/amt-13-2797-2020

Hu, M., Yu, Z., Griffis, T. J., Yang, W. H., Mohn, J., Millet, D. B., et al. (2024). Hydrologic connectivity regulates riverine N_2O sources and dynamics. *Environmental Science & Technology*, *58*(22), 9701–9713. https://doi.org/10.1021/acs.est.4c01285

Keeling, C. D. (1958). The concentration and isotopic abundances of atmospheric carbon dioxide in rural areas. *Geochimica et Cosmochimica Acta*, *13*(4), 322–334. https://doi.org/10.1016/0016-7037(58)90033-4

Kim, S. Y., Millet, D. B., Hu, L., Mohr, M. J., Griffis, T. J., Wen, D., et al. (2013). Constraints on carbon monoxide emissions based on tall tower measurements in the U.S. upper midwest. *Environmental Science and Technology*, *47*(15), 130725095602007. https://doi.org/10.1021/es4009486

Kort, E. A., Eluszkiewicz, J., Stephens, B. B., Miller, J. B., Gerbig, C., Nehrkorn, T., et al. (2008). Emissions of CH_4 and N_2O over the United States and Canada based on a receptor-oriented modeling framework and COBRA-NA atmospheric observations. *Geophysical Research Letters*, *35*(18). https://doi.org/10.1029/2008GL034031

Lawrence, N. C., Tenesaca, C. G., VanLoocke, A., & Hall, S. J. (2021). Nitrous oxide emissions from agricultural soils challenge climate sustainability in the US Corn Belt. *Proceedings of the National Academy of Sciences of the United States of America*, *118*(46), e2112108118. https://doi.org/10.1073/pnas.2112108118j1of8

Lewicka-Szczebak, D., Dyckmans, J., Kaiser, J., Marca, A., Augustin, J., & Well, R. (2016). Oxygen isotope fractionation during N_2O production by soil denitrification. *Biogeosciences*, *13*, 1129–1144. https://doi.org/10.5194/bg-13-1129-2016

Liang, Q., Nevison, C., Dlugokencky, & E., Hall, B. D., & Dutton, G. (2022). 3-D atmospheric modeling of the global budget of N_2O and its Isotopologues.pdf. *Global Biogeochemical Cycles*, *36*(e2021GB007202). https://doi.org/10.1029/2021GB007202

Lu, C., Yu, Z., Zhang, J., Cao, P., Tian, H., & Nevison, C. (2022). Century-long changes and drivers of soil nitrous oxide (N_2O) emissions across the contiguous United States. *Global Change Biology*, *28*(7), 2505–2524. https://doi.org/10.1111/gcb.16061

Miller, J. B., & Tans, P. P. (2003). Calculating isotopic fractionation from atmospheric measurements at various scales. *Tellus Series B Chemical and Physical Meteorology*, *55*(2), 207–214. https://doi.org/10.1034/j.1600-0889.2003.00020.x

Miller, S. M., Kort, E. A., Hirsch, A. I., Dlugokencky, E. J., Andrews, A. E., Xu, X., et al. (2012). Regional sources of nitrous oxide over the United States: Seasonal variation and spatial distribution. *Journal of Geophysical Research*, *117*(D6). https://doi.org/10.1029/2011JD016951

Mohn, J., Biasi, C., Bode, S., Boeckx, P., Brewer, P. J., Eggleston, S., et al. (2022). Isotopically characterised N_2O reference materials for use as community standards. *Rapid Communications in Mass Spectrometry*, *36*(13). https://doi.org/10.1002/rcm.9296

Montzka, S. A., Dlugokencky, E. J., & Butler, J. H. (2011). Non-CO_2 greenhouse gases and climate change. *Nature*, *476*(7358), 43–50. https://doi.org/10.1038/nature10322

Ogawa, M., & Yoshida, N. (2005). Nitrous oxide emission from the burning of agricultural residue. *Atmospheric Environment*, *39*(19), 3421–3429. https://doi.org/10.1016/j.atmosenv.2005.01.059

Ostrom, N. E., Gandhi, H., Coplen, T. B., Toyoda, S., Bohlke, J. K., Brand, W. A., et al. (2018). Preliminary assessment of stable nitrogen and oxygen isotopic composition of USGS51 and USGS52 nitrous oxide reference gases and perspectives on calibration needs. *Rapid Communications in Mass Spectrometry*, *32*(15), 1207–1214. https://doi.org/10.1002/rcm.8157

Ostrom, N. E., & Ostrom, P. H. (2017). Mining the isotopic complexity of nitrous oxide: A review of challenges and opportunities. *Biogeochemistry*, *132*(3), 359–372. https://doi.org/10.1007/s10533-017-0301-5

Park, S., Croteau, P., Boering, K. a., Etheridge, D. M., Ferretti, D., Fraser, P. J., et al. (2012). Trends and seasonal cycles in the isotopic composition of nitrous oxide since 1940. *Nature Geoscience*, *5*(4), 261–265. https://doi.org/10.1038/ngeo1421

Ravishankara, A. R., Daniel, J. S., & Portmann, R. W. (2009). Nitrous oxide (N_2O): The dominant ozone-depleting substance emitted in the 21st century. *Science*, *326*(October), 123–125. https://doi.org/10.1126/science.1176985

Snider, D., Thompson, K., Wagner-Riddle, C., Spoelstra, J., & Dunfield, K. (2015). Molecular techniques and stable isotope ratios at natural abundance give complementary inferences about N_2O production pathways in an agricultural soil following a rainfall event. *Soil Biology and Biochemistry*, *88*, 197–213. https://doi.org/10.1016/j.soilbio.2015.05.021

Snider, D. M., Venkiteswaran, J. J., Schiff, S. L., & Spoelstra, J. (2015). From the ground up: Global nitrous oxide sources are constrained by stable isotope values. *PLoS One*, *10*(3), e0118954. https://doi.org/10.1371/journal.pone.0118954

Sutka, R., Ostrom, N., Ostrom, P., Breznak, J., Gandhi, H., Pitt, A., & Li, F. (2006). Distinguishing nitrous oxide production from nitrification and denitrification on the basis of isotopomer abundances. *Applied and Environmental Microbiology*, *72*(1), 638–644. https://doi.org/10.1128/AEM.72.1.638-644.2006

Tian, H., Xu, R., Canadell, J. G., Thompson, R. L., Winiwarter, W., Suntharalingam, P., et al. (2020). A comprehensive quantification of global nitrous oxide sources and sinks. *Nature*, *586*(7828), 248–256. https://doi.org/10.1038/s41586-020-2780-0

Toyoda, S., & Yoshida, N. (1999). Determination of nitrogen isotopomers of nitrous oxide on a modified isotope ratio mass spectrometer. *Analytical Chemistry*, *71*(20), 4711–4718. https://doi.org/10.1021/ac9904563

Toyoda, S., Yoshida, N., & Koba, K. (2017). Isotopocule analysis of biologically produced nitrous oxide in various environments. *Mass Spectrometry Reviews*, *36*(2), 135–160. https://doi.org/10.1002/mas.21459

Turner, P. A., Griffis, T. J., Baker, J. M., Lee, X., Crawford, J. T., Loken, L. C., & Venterea, R. T. (2016). Regional-scale controls on dissolved nitrous oxide in the Upper Mississippi River. *Geophysical Research Letters*, *43*(9), 4400–4407. https://doi.org/10.1002/2016GL068710

Turner, P. A., Griffis, T. J., Lee, X., Baker, J. M., Venterea, R. T., Wood, J. D., & Del Grosso, S. J. (2015). Indirect nitrous oxide emissions from streams within the US Corn Belt scale with stream order. *Proceedings of the National Academy of Sciences of the United States of America*, *112*(32), 9839–9843. https://doi.org/10.1073/pnas.1503598112

Wagner-Riddle, C., Congreves, K. A., Abalos, D., Berg, A. A., Brown, S. E., Ambadan, J. T., et al. (2017). Globally important nitrous oxide emissions from croplands induced by freeze–thaw cycles. *Nature Geoscience*, *10*(4), 279–283. https://doi.org/10.1038/ngeo2907

Wang, L., Caylor, K. K., Villegas, J. C., Barron-Gafford, G. A., Breshears, D. D., & Huxman, T. E. (2010). Partitioning evapotranspiration across gradients of woody plant cover: Assessment of a stable isotope technique. *Geophysical Research Letters*, *37*(9), L09401. https://doi.org/10.1029/2010gl043228

Wolf, B., Merbold, L., Decock, C., Tuzson, B., Harris, E., Six, J., et al. (2015). First on-line isotopic characterization of N_2O above intensively managed grassland. *Biogeosciences*, *12*(8), 2517–2531. https://doi.org/10.5194/bg-12-2517-2015

Yu, L., Harris, E., Henne, S., Eggleston, S., Steinbacher, M., Emmenegger, L., et al. (2020). The isotopic composition of atmospheric nitrous oxide observed at the high-altitude research station Jungfraujoch, Switzerland. *Atmospheric Chemistry and Physics*, *20*(11), 6495–6519. https://doi.org/10.5194/acp-20-6495-2020

Yu, L., Harris, E., Lewicka-Szczebak, D., Barthel, M., Blomberg, M. R. A., Harris, S. J., et al. (2020). What can we learn from N_2O isotope data? - Analytics, processes and modelling. *Rapid Communications in Mass Spectrometry*, *34*(20). https://doi.org/10.1002/rcm.8858

Yu, Z., Hu, Y., Gentry, L. E., Yang, W. H., Margenot, A. J., Guan, K., et al. (2023). Linking water age, nitrate export regime, and nitrate isotope biogeochemistry in a tile-drained agricultural field. *Water Resources Research*, *59*(12), e2023WR034948. https://doi.org/10.1029/2023wr034948

References From the Supporting Information

Burzaco, J. P., Smith, D. R., & Vyn, T. J. (2013). Nitrous oxide emissions in Midwest US maize production vary widely with band-–injected N fertilizer rates, timing and nitrapyrin presence. *Environmental Research Letters*, *8*(3), 035031. https://doi.org/10.1088/1748-9326/8/3/035031

Cates, R., & Keeney, D. (1987). Nitrous-oxide production throughout the year from fertilized and manured maize fields. *Journal of Environmental Quality*, *16*(4), 443–447. https://doi.org/10.2134/Jeq1987.00472425001600040026x

Chen, Z., Griffis, T. J., Baker, J. M., Millet, D. B., Wood, J. D., Dlugokencky, E. J., et al. (2018). Source partitioning of methane emissions and its seasonality in the U.S. Midwest. *Journal of Geophysical Research: Biogeosciences*. https://doi.org/10.1002/2017JG004356

Evaristo, J., Jasechko, S., & McDonnell, J. J. (2015). Global separation of plant transpiration from groundwater and streamflow. *Nature*, *525*(7567), 91–94.

Fassbinder, J. J., Schultz, N. M., Baker, J. M., & Griffis, T. J. (2013). Automated, low-power chamber system for measuring N_2O emissions. *Journal of Environmental Quality*, *42*, 606–614.

Fernandez, F. G., Terry, R. E., & Coronel, E. G. (2015). Nitrous oxide emissions from anhydrous ammonia, urea, and polymer-coated urea in Illinois Cornfields. *Journal of Environmental Quality*, *44*(2), 415–422. https://doi.org/10.2134/jeq2013.12.0496

Fernandez, F. G., Venterea, R. T., & Fabrizzi, K. P. (2016). Corn nitrogen management influences nitrous oxide emissions in drained and undrained soils. *Journal of Environmental Quality*, *45*(6), 1847–1855. https://doi.org/10.2134/jeq2016.06.0237

Frame, C. H., & Casciotti, K. L. (2010). Biogeochemical controls and isotopic signatures of nitrous oxide production by a marine ammonia-oxidizing bacterium. *Biogeosciences*, *7*(9), 2695–2709. https://doi.org/10.5194/bg-7-2695-2010

Good, S. P., Noone, D., & Bowen, G. (2015). Hydrologic connectivity constrains partitioning of global terrestrial water fluxes. *Science*, *349*(6244), 175–177.

Hall, S. J., Weintraub, S. R., & Bowling, D. R. (2016). Scale-dependent linkages between nitrate isotopes and denitrification in surface soils: implications for isotope measurements and models. *Oecologia*, *181*, 1221–1231.

Jarecki, M. K., Parkin, T. B., Chan, A. S. K., Hatfield, J. L., & Jones, R. (2008). Comparison of DAYCENT-simulated and measured nitrous oxide emissions from a corn field. *Journal of Environmental Quality*, *37*(5), 1685–1690. https://doi.org/10.2134/jeq2007.0614

Jin, V. L., Baker, J. M., Johnson, J. M.-F., Karlen, D. L., Lehman, R. M., Osborne, S. L., et al. (2014). Soil Greenhouse Gas Emissions in Response to Corn Stover Removal and Tillage Management Across the US Corn Belt. *Bioenergy Research*, *7*(2), 517–527. https://doi.org/10.1007/s12155-014-9421-0

Kaiser, J., Rockmann, T., & Brenninkmeijer, C. (2003). Complete and accurate mass spectrometric isotope analysis of tropospheric nitrous oxide. *Journal of Geophysical Research-Atmospheres*, *108*(D15). https://doi.org/10.1029/2003JD003613

Kelly, C. L., Travis, N. M., Baya, P. A., & Casciotti, K. L. (2021). Quantifying nitrous oxide cycling regimes in the eastern tropical north Pacific Ocean with isotopomer analysis. *Global Biogeochemical Cycles*, *35*(2). https://doi.org/10.1029/2020GB006637

Klaus, J., Zehe, E., Elsner, M., Külls, C., & McDonnell, J. J. (2013). Macropore flow of old water revisited: experimental insights from a tile-drained hillslope. *Hydrology and Earth System Sciences*, *17*(1), 103–118.

Knighton, J., Souter-Kline, V., Volkmann, T., Troch, P.A., Kim, M., Harman, C.J., et al. (2019). Seasonal and topographic variations in eco-hydrological separation within a small, temperate, snow-influenced catchment. *Water Resources Research*, *55*(8), 6417–6435.

Maharjan, B., & Venterea, R. T. (2014). Anhydrous ammonia injection depth does not affect nitrous oxide emissions in a Silt Loam over two growing seasons. *Journal of Environmental Quality*, *43*(5), 1527–1535. https://doi.org/10.2134/jeq2014.07.0292

McDonnell, J. J. (2014). The two water worlds hypothesis: ecohydrological separation of water between streams and trees? *Wiley Interdisciplinary Reviews: Water*, *1*(4), 323–329.

Nash, P. R., Motavalli, P. P., & Nelson, K. A. (2012). Nitrous oxide emissions from Claypan soils due to nitrogen fertilizer source and tillage/fertilizer placement practices. *Soil Science Society of America Journal*, *76*(3), 983–993. https://doi.org/10.2136/sssaj2011.0296

Omonode, R. A., Smith, D. R., Gal, A., & Vyn, T. J. (2011). Soil nitrous oxide emissions in corn following three decades of tillage and rotation treatments. *Soil Science Society of America Journal*, *75*(1), 152–163. https://doi.org/10.2136/sssaj2009.0147

Omonode, R. A., Kovacs, P., & Vyn, T. J. (2015). Tillage and nitrogen rate effects on area- and yield-scaled nitrous oxide emissions from pre-plant anhydrous ammonia. *Agronomy Journal*, *107*(2), 605–614. https://doi.org/10.2134/agronj14.0440

Opdyke, M. R., Ostrom, N. E., & Ostrom, P. H. (2009). Evidence for the predominance of denitrification as a source of N_2O in temperate agricultural soils based on isotopologue measurements. *Global Biogeochemical Cycles*, *23*(4). https://doi.org/10.1029/2009gb003523

Ostrom, N. E., Sutka, R., Ostrom, P. H., Grandy, A. S., Huizinga, K. M., Gandhi, H., et al. (2010). Isotopologue data reveal bacterial denitrification as the primary source of N_2O during a high flux event following cultivation of a native temperate grassland. *Soil Biology and Biochemistry*, *42*(3), 499–506. https://doi.org/10.1016/j.soilbio.2009.12.003

Ostrom, P. H., DeCamp, S., Gandhi, H., Haslun, J., & Ostrom, N. E. (2021). The influence of tillage and fertilizer on the flux and source of nitrous oxide with reference to atmospheric variation using laser spectroscopy. *Biogeochemistry*, *152*(2–3), 143–159. https://doi.org/10.1007/s10533-020-00742-y

Parkin, T., & Kaspar, T. (2006). Nitrous oxide emissions from corn-soybean systems in the Midwest. *Journal of Environmental Quality*, *35*, 1496–1506.

Renée Brooks, J., Barnard, H. R., Coulombe, R., & McDonnell, J. J. (2010). Ecohydrologic separation of water between trees and streams in a Mediterranean climate. *Nature Geoscience*, *3*(2), 100–104.

Smith, D. R., Hernandez-Ramirez, G., Armstrong, S. D., Bucholtz, D. L., & Stott, D. E. (2011). Fertilizer and tillage management impacts on non-carbon-dioxide greenhouse gas emissions. *Soil Science Society of America Journal*, *75*(3), 1070–1082. https://doi.org/10.2136/sssaj2009.0354

Sprenger, M., Leistert, H., Gimbel, K., & Weiler, M. (2016). Illuminating hydrological processes at the soil-vegetation-atmosphere interface with water stable isotopes. *Reviews of Geophysics*, *54*(3), 674–704.

Sprenger, M., Stumpp, C., Weiler, M., Aeschbach, W., Allen, S. T., Benettin, P., et al. (2019). The demographics of water: A review of water ages in the critical zone. *Reviews of Geophysics*, *57*(3), 800–834.

Swaney, D. P., Howarth, R. W., & Hong, B. (2018). Nitrogen use efficiency and crop production: Patterns of regional variation in the United States, 1987–2012. *Science of the Total Environment*, *635*, 498–511.

Turner, P. A., Baker, J. M., Griffis, T. J., & Venterea, R. T. (2016). Impact of Kura Clover Living Mulch on Nitrous Oxide Emissions in a Corn–Soybean System. *Journal of Environment Quality*, *45*(5), 1782. https://doi.org/10.2134/jeq2016.01.0036

Venterea, R. T., & Coulter, J. A. (2015). Split application of urea does not decrease and may increase nitrous oxide emissions in rainfed corn. *Agronomy Journal*. https://doi.org/10.2134/agronj14.0411

Venterea, R. T., Dolan, M. S., & Ochsner, T. E. (2010). Urea Decreases Nitrous Oxide Emissions Compared with Anhydrous Ammonia in a Minnesota Corn Cropping System. *Soil Science Society of America Journal*, *74*(2), 407. https://doi.org/10.2136/sssaj2009.0078

Venterea, R. T., Coulter, J. A., & Dolan, M. S. (2016). Evaluation of intensive "4R" strategies for decreasing nitrous oxide emissions and nitrogen surplus in rainfed corn. *Journal of Environmental Quality*, *45*(4), 1186–1195. https://doi.org/10.2134/jeq2016.01.0024

Weigand, M. A., Foriel, J., Barnett, B., Oleynik, S., & Sigman, D. M. (2016). Updates to instrumentation and protocols for isotopic analysis of nitrate by the denitrifier method. *Rapid Communications in Mass Spectrometry*, *30*(12), 1365–1383. https://doi.org/10.1002/rcm.7570

Werle, P., Mucke, R., & Slemr, F. (1993). The limits of signal averaging in atmospheric trace-gas monitoring by Tunable Diode-Laser Absorption-Spectroscopy (TDLAS). *Applied Physics B-Photophysics and Laser Chemistry*, *57*, 131–139.

Werle, P. (2011). Accuracy and precision of laser spectrometers for trace gas sensing in the presence of optical fringes and atmospheric turbulence. *Applied Physics B: Lasers and Optics*, *102*, 313–329.

Westley, M. B., Popp, B. N., & Rust, T. M. (2007). The calibration of the intramolecular nitrogen isotope distribution in nitrous oxide measured by isotope ratio mass spectrometry. *Rapid Communications in Mass Spectrometry*, *21*(3), 391–405. https://doi.org/10.1002/rcm.2828

Williams, M. R., King, K. W., Ford, W., Buda, A. R., & Kennedy, C. D. (2016). Effect of tillage on macropore flow and phosphorus transport to tile drains. *Water Resources Research*, *52*(4), 2868–2882.